Assessment of the Mars 2020 Entry, Descent, and Landing Simulation

David W. Way*, Soumyo Dutta†, Carlie H. Zumwalt‡, David J. Blette§
NASA Langley Research Center, Hampton, VA 23681, USA

On February 18, 2021, the Mars 2020 Perseverance rover and Ingenuity helicopter successfully landed inside Jezero Crater. At 1026 kg, Perseverance is the largest, most sophisticated rover ever delivered to another planet. This event marked the ninth successful landing and fifth rover to be delivered at Mars. The Program to Optimize Simulated Trajectories II (POST2), a trajectory simulation tool, was the prime entry, descent, and landing (EDL) performance simulation for Mars 2020. This paper presents a few initial comparisons between EDL flight telemetry and the simulation predictions. In general, approximately 90% of the EDL as-flown values were within $\pm 3\sigma$ (standard deviations) of the pre-flight simulation predictions, and the the anomalies are discussed in the paper. These comparisons are important in order to understand how each of the individual models and the integrated simulation as a whole performed. This information is fed forward to future missions, which benefit from the knowing where additional resources or study are needed and where uncertainties may be reduced to enable improved performance.

Nomenclature

β	Ballistic coefficient	F^{-1}	Inverse cumulative distribution function
ρ	Density	P	Pressure
σ	Standard deviation	Q	Quantile
h	Altitude	R	Gas constant
$\dot{h}$	Altitude rate	T	Temperature
n	Number of samples	$\dot{V}$	Deceleration
p	Percentage	$\ddot{V}$	Jerk
q	Dynamic pressure	X	Flight value of metric of interest
x	Value from simulation of metric of interest		

I. Introduction

The Mars 2020 mission delivered the 1026 kg Perservance rover and the 2 kg Ingenuity helicopter to the surface of Mars on Feb. 18th, 2021. The mission was the largest and most sophisticated mission to the Red planet to date, and was the ninth successful landing on the planet. The Mars 2020 mission built upon the successful Mars Science Laboratory (MSL) mission from 2012, and its entry, descent, and landing (EDL) sequence was very similar to the previous mission, as seen in Figure 1, which also shows the as-flown conditions from Mars 2020. Mars 2020 incorporated two major EDL technologies that enabled landing the rover in a site too hazardous for previous missions. These technologies - range trigger [1, 2] and Terrain Relative Navigation (TRN) [3] - enabled the potential landing ellipse to be smaller by several kilometers and the vehicle to divert to safe zones on the map due to better knowledge of its position during flight.

Throughout the EDL system development lifecycle, simulation predictions are used to assist the EDL systems engineering team in: drafting sub-system requirements, making design choices, understanding system sensitivities, identifying vulnerabilities, validating system requirements through analysis, establishing flight software parameters, and making in-flight operational recommendations. The purpose of the simulation is to model the flight in sufficient detail

*Aerospace Engineer, Atmospheric Flight and Entry Systems Branch, 1 N. Dryden St., M/S 489, and AIAA Member.
†Aerospace Engineer, Atmospheric Flight and Entry Systems Branch, 1 N. Dryden St., M/S 489, and Senior AIAA Member.
‡Aerospace Engineer, Atmospheric Flight and Entry Systems Branch, 1 N. Dryden St., M/S 489, and AIAA Member.
§Aerospace Engineer, Atmospheric Flight and Entry Systems Branch, 1 N. Dryden St., M/S 489, and AIAA Member.

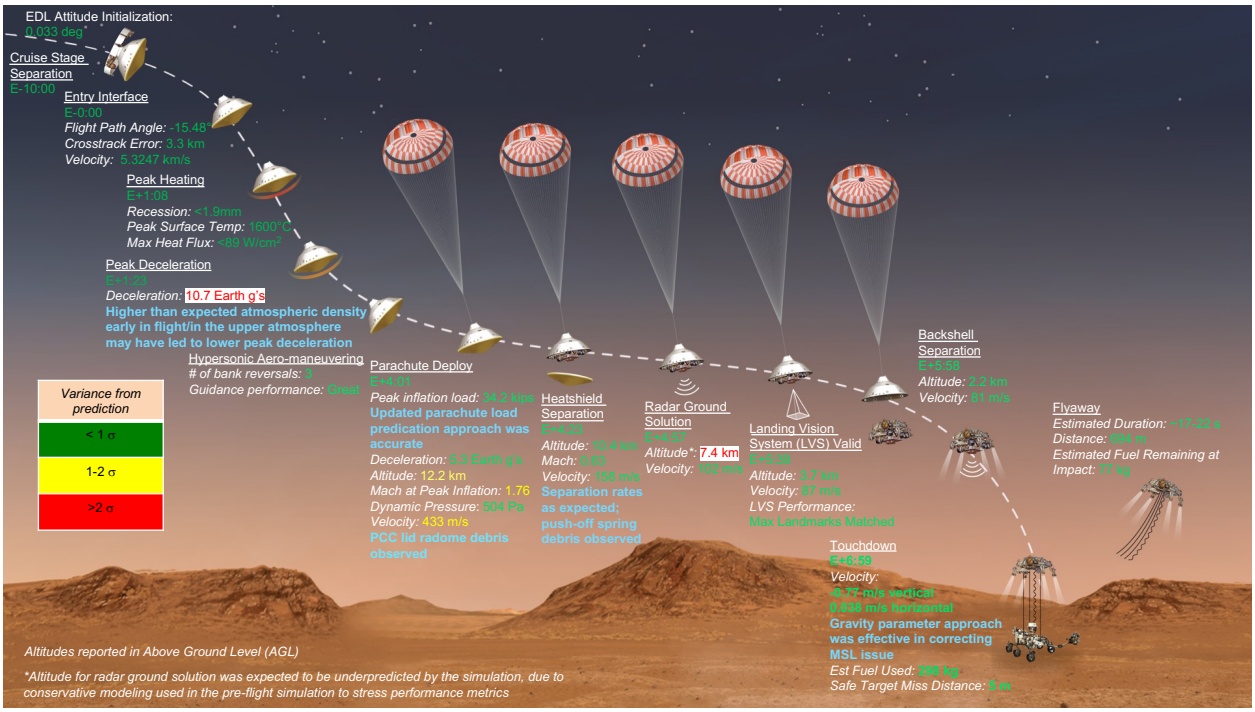

Fig. 1 Mars 2020 EDL concept of operations and as-flown conditions.

and with sufficient accuracy, that the systems engineering team can correctly evaluate the EDL system performance when performing these tasks.

The purpose of this paper is not to reconstruct the flight path of the vehicle on Feb. 18th, 2021. The team relies on the analysis presented in other papers to establish the as-flown trajectory, specifically the Best Estimated Trajectory (BET) developed by the Guidance, Navigation, and Controls (GNC) team [4] and the reconstruction using a post-flight Extended Kalman Filter (EKF) tool [5]. Nor is the purpose to identify an individual case within the Monte Carlo (MC) that most closely matches those as-flown values, or to re-tune the simulation so that it matches better the flight trajectory.

The purpose of this paper is to evaluate the predictive power of the end-to-end EDL simulation that was used throughout EDL system development and EDL approach operations, prior to landing. The intent is to answer the question, “How well did the simulation predict the observed flight environments?" by directly comparing as-flown flight metrics with their equivalent pre-flight predictions. These comparisons allow the team to identify anomalies, make inferences about the veracity of individual simulation models, and potentially to assess the over-all level of conservatism in the simulation.

The simulation used for the comparisons presented in this section is the official configuration-controlled version of the simulation (v.2021.Bravo) used during final EDL approach operations, initialized with the navigation team’s final delivery of entry states (OD138). All of the source code, models, model input parameters, and Monte Carlo uncertainties are unchanged from those used to produce the final predictions prior to landing. It is important for providing a candid evaluation that we are not leveraging any post-flight knowledge to improve these comparisons.

II. Simulation Detail

The Program to Optimize Simulated Trajectories II (POST2) is the tool used for end-to-end EDL simulations for the Mars 2020 mission. POST2 is a six degree-of-freedom flight dynamics simulation tool that can simultaneously simulate the trajectory of up to 20 independent or connected rigid bodies. It is a generalized point mass, discrete-parameter targeting and optimization trajectory simulation program with multi-vehicle capabilities that integrates translational and rotational equations of motion along the trajectory. The simulation tool has significant EDL flight heritage as it has been used in the past successfully for several Mars EDL missions, such as Mars Pathfinder [6], Mars Exploration Rovers [7], Mars Phoenix [8], Mars Science Laboratory [9], and Mars InSight [10].

The Mars 2020 simulation is a continuation of the POST2-based MSL end-to-end EDL simulation developed at the

NASA Langley Research Center. The simulation starts approximately 50 s after Cruise Stage Separation and models the trajectories of fourteen independent bodies, such as the descent stage, parachute, backshell, heatshield, rover, and the ejected balance masses. Interaction between interconnected bodies, such as the parachute and the aeroshell or the descent stage and the rover, are modeled using multi-body force models originally developed for the Mars Exploration Rovers' simulations [7, 9].

The end-to-end simulation, which incorporates vehicle, planet, and atmospheric models, is used during mission planning to assess the system's performance against requirements and response to off-nominal conditions. In order to quantify the robustness of the system, Monte Carlo analysis is conducted using the simulation. A pre-set group of input variables are stochastically dispersed and statistics on metrics of interest are tracked at specific EDL events. The simulation uses site specific atmospheric parameters – density, temperature, pressure, and horizontal winds – generated by mesoscale atmospheric models [11]. The use of a physics-based atmospheric profiles, such as mesoscale based data, in the simulation was novel to MSL and the Mars 2020 simulation continues that usage. The output metrics are collected for multiple runs of the simulation.

In this paper, the pre-flight predictions from this end-to-end simulation is compared with flight data and reconstruction.

III. Footprint Performance

For Mars 2020, the final landing location is selected in real-time by the TRN system to maximize the likelihood of a safe landing. This location can be up to 635 m from the estimated "zero-divert" location, or the point at which the spacecraft diverts away from the backshell and toward the targeted point. Therefore, the performance of the entry targeting is measured with respect to the zero-divert location, rather than the final landed location.

Figure 2 shows the as-flown point along with the pre-flight 1σ, 2σ, and 3σ footprints of the zero-divert location. The location of the as-flown zero-divert point was 1.134 km southeast of the pre-flight target, and was a 1.03 σ quantile with respect to pre-flight predictions, making this the most accurately targeted Mars landing to date. The values for the actual Perseverance landing site, known as Octavia E. Butler Landing, was determined based on High Resolution Imaging Science Experiment (HiRISE) imagery of the landed rover. The HiRISE inertial map-tie error is expected to be on the order of 50 m.

In addition, HiRISE was able to observe other EDL hardware components, like the backshell and heatshield, and their final resting locations was determined from the post-landing imagery. Table 1 provides the location of these hardware components as well as other points of interest, along with their ranges from the landed rover location. Relative measurements between each of the components can be used to compare with simulation predictions of the flight of these separated components. The pre-entry target is the location used pre-flight as the landing location and was used to center the pre-flight landing ellipse. During flight prior to backshell separation, Mars 2020 did not try to target the pre-entry target since Mars 2020 was not attempting pin-point landing. Instead, Mars 2020 was attempting safe landing using TRN and chose the safest landing point in two wedges left or right of the predominant direction it was moving at backshell separation. The chosen and the opposite wedge targets show these two potential in-flight targets that Mars 2020 was choosing between.

Table 1 Photographic Localizations based on HiRISE Imagery.

	Latitude (deg)	Longitude (deg)	Range from Landed Rover (m)
Landed Rover	18.44463	77.45088	0.00
Chosen Target	18.44468	77.45081	4.75
Backshell & Parachute	18.45160	77.43216	1129.29
Descent Stage	18.45209	77.44193	668.92
Heatshield	18.45533	77.47444	1466.87
Zero Divert Point	18.45194	77.44316	612.82
Opposite Wedge Target	18.46089	77.43942	1158.27
Pre-Entry Target	18.46630	77.42980	1745.60

Figure 3 compares the actual heatshield impact point to the predicted location, given the as-flown heatshield separation (HSS) location, along with the pre-flight 1σ, 2σ, and 3σ footprints. The predicted location shown is calculated by applying the relative position of heatshield impact, with respect to HSS, to the as-flown HSS location – as

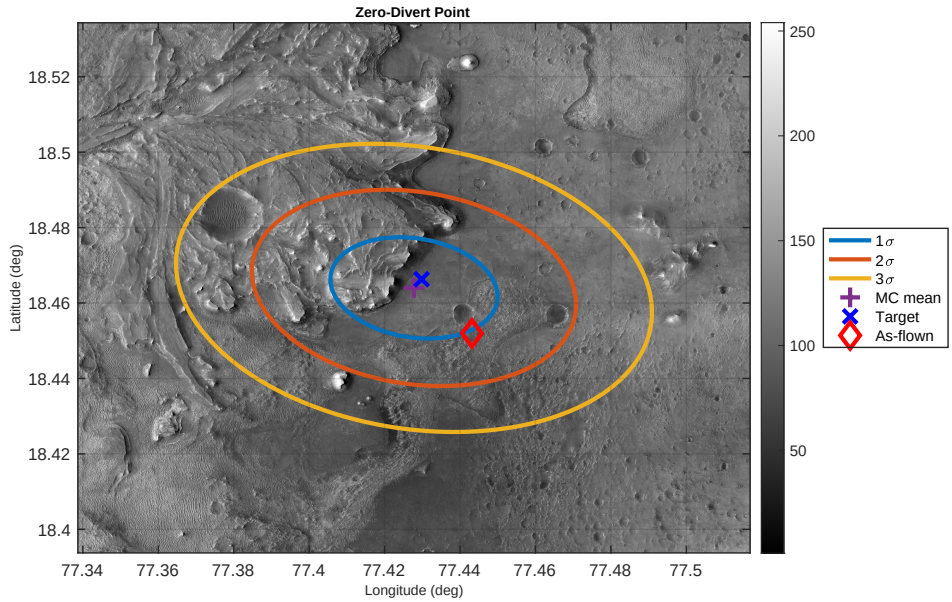

Fig. 2 Comparison of actual zero-divert location, indicated by the red diamond marker, to Monte Carlo predictions from OD230 orbit determination solution. The three ellipses shown are a 98.89%- tile ellipse, which is the cumulative probability of 3.0σ for a Rayleigh distribution; a 86.47%-tile ellipse (2.0σ), and a 39.35%-tile ellipse (1.0σ).

determined by the GN&C backwards propagation reconstruction. This comparison demonstrates the accuracy of the modeled post-separation flight of the heatshield, which is observed to be quite good (0.34 σ).

Likewise, Figure 4 compares the actual backshell impact point (labeled as as-flown) along with the pre-flight 1σ, 2σ, and 3σ footprints. The zero-divert location is also shown for comparison, since backshell separation occurs at this point. This comparison demonstrates the accuracy of the modeled post-separation flight of the backshell and parachute. The Gaussian quantile of this comparison is 1.72 σ. Given the difficulty in modeling the post-separation flight of the lightly-loaded parachute, which is highly affected by assumed wind models, the level of agreement is unsurprising.

Figure 5 compares the actual descent stage impact point to the predicted location, given the as-flown touchdown location. The predicted location shown is calculated by applying the relative position of descent stage impact, with respect to the touchdown point, to the as-flown landing location. This comparison demonstrates the accuracy of the modeled post-landing flyaway of the descent stage. The Gaussian quantile of this comparison, based on range flown, is 2.12σ, which is quite high. Figure 6 shows the statistical comparison of the predicted fly-away distance with the 669 m as-flown value. This observation is one of the indicators which led to the identification of the Main Lander Engine (MLE) over-performance anomaly, discussed in Section V.D.

Finally, Figure 7 shows the predicted locations of various entry, descent, and landing events and the as-flown locations of those events. One can see that from SUFR down to the backshell separation (zero-divert point) location, the spacecraft was close to the +1σ boundary of the predictions at these events.

IV. Statistical Comparison

The following section compiles reconstructed as-flown quantities from various sources and compares each value to the equivalent 8001 simulation samples captured in the pre-flight Monte Carlo. This comparison is expressed as an equivalent standard Gaussian quantile, measured in non-dimensional standard deviations (σ). In a quantile-quantile plot, this metric is the x-coordinate that would be associated with a y-coordinate equal to the observed flight value – given the distribution predicted by the simulation. The value can be calculated from Equation 1, where the quantile (Q) is equal to the inverse Cumulative Distribution Function (CDF) (F^{-1}) of the percentage (p) of simulation cases (x) that are less than the flight value (X), given n simulation cases. For any continuous variable x, this can equivalently be calculated using Equation 2, where p is found from the percent of cases that exceed X. For discrete variables, where many simulation cases can share the same value, Equations 1 and 2 can produce different results. In these cases, the

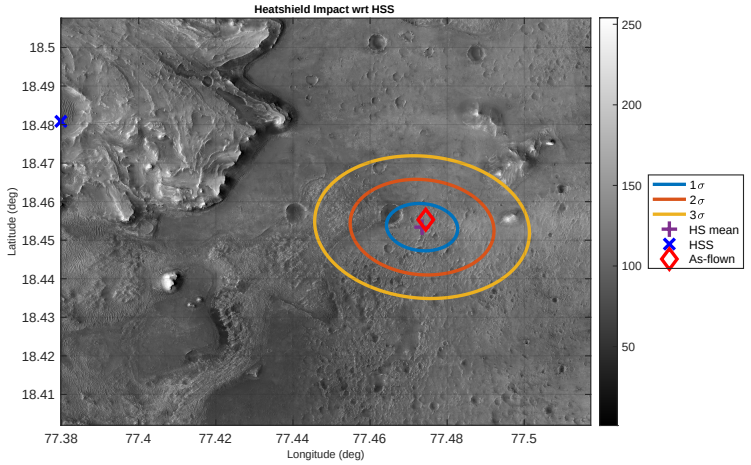

Fig. 3 Heatshield Impact, Given Heatshield Separation Location.

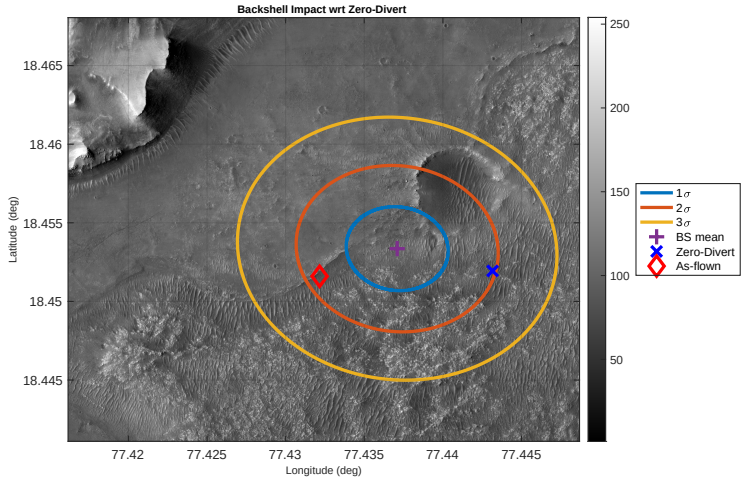

Fig. 4 Backshell Impact, Given Zero-Divert Location.

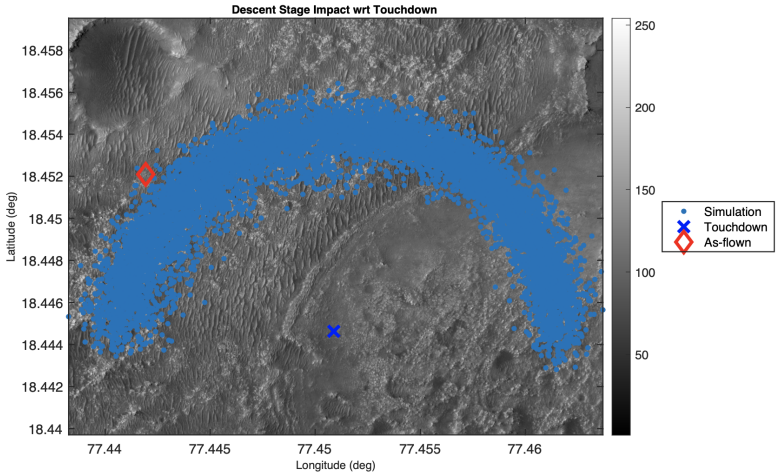

Fig. 5 Descent Stage Impact, Given Landed Location.

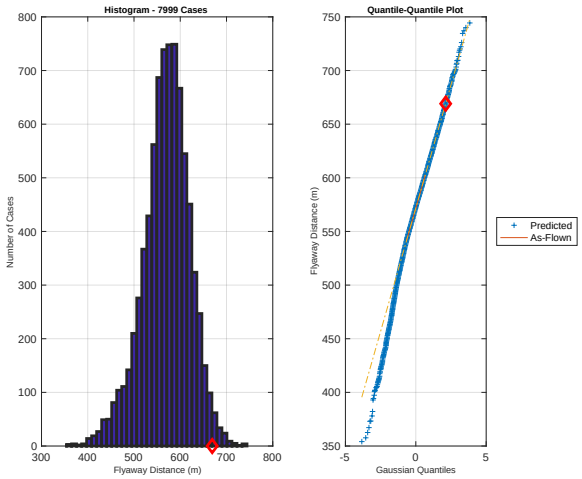

Fig. 6 Flyaway Distance.

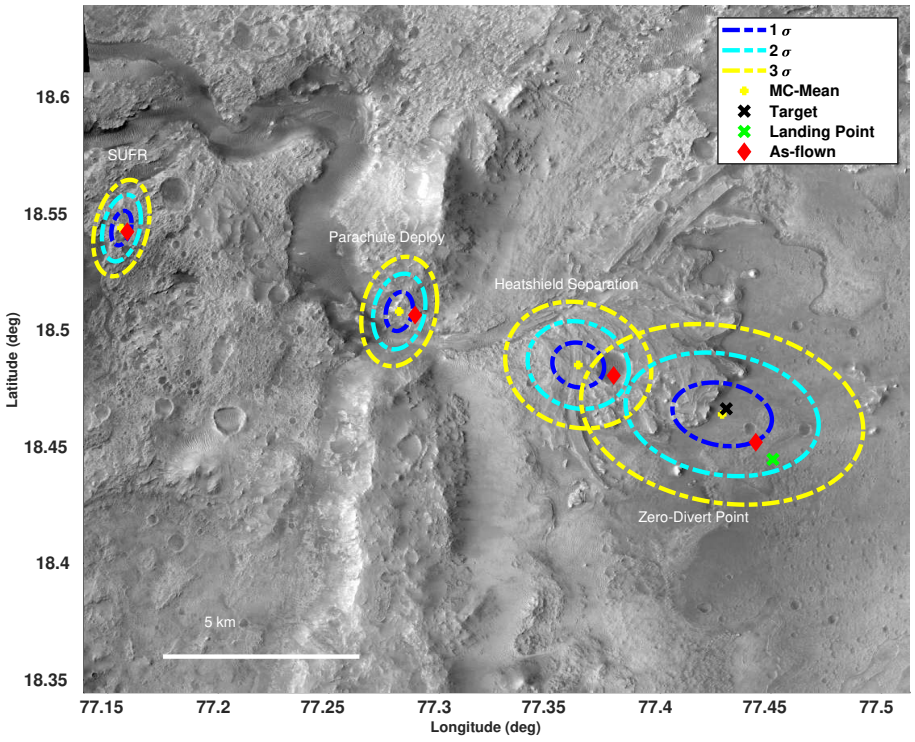

Fig. 7 Prediction trajectory snapshots and as-flown location for various entry, descent, and landing events.

result closest to median of the distribution is reported – or 0.0 σ if the two results straddle the median.

$$Q = F^{-1}\left(p = \frac{x < X}{n}\right) \tag{1}$$

$$Q = F^{-1}\left(p = 1 - \frac{x > X}{n}\right) \tag{2}$$

Special cases also result when the flight value exceeds the minimum or maximum from the simulation predictions. When $X < min(x)$, then $Q = F^{-1}(0) = -\infty$, and when $X > max(x)$, then $q = F^{-1}(1) = \infty$. However, the simulation extrema are limited by the number of samples n in the Monte Carlo, such that the minimum and maximum quantiles are determined from $p_{min} = 0.5/n$ and $p_{max} = (n - 0.5)/n$, respectively. Therefore, for an 8001 case Monte Carlo, the quantile is reported as "$< -3.836\ \sigma$" when $X < min(x)$ and "$> 3.836\ \sigma$" when $X > max(x)$. These situations, when they occur, are of particular interest, as they represent cases where the observed flight metric was outside the range of pre-flight predicted conditions. This is expected to randomly occur very rarely. Typically, such observations point to systemic errors in the simulation models.

A. Overall Statistical Performance

More than 1000 metrics from various reconstruction sources are presented in Section IV, along with their calculated Gaussian quantile. Table 2 below provides a summary of these quantiles.

Table 2 Summary of All Comparisons

Range	Std. Normal	Count	Percentage
$\|\sigma\| > 3.84$	0.012%	115 of 1170	9.83%
$3 < \|\sigma\| < 3.84$	0.258%	15 of 1170	1.28%
$1.5 < \|\sigma\| < 3$	13.091%	92 of 1170	7.86%
$\|\sigma\| < 1.5$	86.639%	948 of 1170	81.03%

Particular attention was given to each of the 115 metrics that exceeded the bounds of the pre-flight predictions and were assigned a quantile "> 3.84", as well as the additional 15 metrics that exceeded 3 σ. Several significant anomalies were identified by examining this group, and their root causes are discussed in Section V.

The remaining 89% of metrics were within $\pm 3\ \sigma$ of simulation predictions. While this statistic is useful for understanding the areas in which the simulation captured the as-flown performance of the spacecraft, it is difficult to draw any additional insights about the conservatism of the simulation from just these statistics alone.

B. Timeline Engine Timepoint Firings

During EDL, the timeline engine is responsible for executing 327 unique timepoints. When each timepoint is executed, the software issues an EDL EVR TIMEPOINT FIRED EVR, similar to the one below.

```
"Fired timepoint=TZERONAV_GNC_START chain=TZERO_NAV_GNC_START anchor=TZERO_NAV action=GNC_START
 (time=666951979.625000 @ srti=40)."
```

In order to compare with simulation results, where SCLK is not used, the elapsed time since TZERO* was used. The firing time of only 114 of these timepoints fall within the scope of time of the Monte Carlo simulation; the rest occur before TZERO or after touchdown. Thus, one can make direct comparisons to pre-flight simulation predictions for only these 114 timepoints. These comparisons are useful for assessing the over-all accuracy of the simulation in predicting the time at which certain events occur. As flight time can vary in different environments (e.g. atmospheric density and winds), these comparisons provide physical constraints on the accuracy of simulation's predictions of those environments. Ref. [12] lists the actual timepoints and their sim comparable, while Table 3 shows the summary comparing the actual time of the timepoints versus their simulation counterpart. As will be discussed in Section V, some of the "$> 3.84\ \sigma$" results are indeed due to mis-predictions in the pre-flight simulation and the causes of some of these cases are discussed. However, some of the differences are due to very small differences in timing that are beyond the intended scope of the simulation. Section V.A also describes a mismatch in how the pre-flight simulation's TZERO

*Specifically, "TZERO TIMELINE": the first 64 Hz sRTI after the EPU commanded time (666951979.51562)

event is initialized as compared to what is done on flight. This mismatch is the origin for some of the $> 3.84\ \sigma$ cases seen in Table 3.

Table 3 Summary of Timepoints Fired Time Comparisons

Range	Std. Normal	Count	Percentage
$\|\sigma\| > 3.84$	0.012%	27 of 114	23.68%
$3 < \|\sigma\| < 3.84$	0.258%	0 of 114	0.00%
$1.5 < \|\sigma\| < 3$	13.091%	0 of 114	0.00%
$\|\sigma\| < 1.5$	86.639%	87 of 114	76.32%

C. GNC Mode Commander State Transitions

During EDL, the GNC main mode commander, a Finite State Machine (FSM), is responsible for transitioning between 38 unique GNC states. Whenever a new state is entered, the mode commander issues an "EDLGNC EVR MC STATE CHANGED" EVR, similar to the one below.

```
"===== Gnc mc new state=MC_DONE at time=666952939.203125 ========================================
 ========="
```

Real-time EVRs provide the as-flown SCLK times of each GNC Mode Commander state change. In order to compare with simulation results where SCLK is not used, the elapsed time since TZERO* is also shown. As the cumulative time spent in each state is captured in the simulation Monte Carlo outputs, direct comparisons to pre-flight simulation predictions can be made. This cumulative time comparison is fundamentally different from the timepoint comparisons above. The timepoints record the total elapsed time and thus reflect the average performance across all previous events. Some of these events may occur early and others late, but only the cumulative effect is captured. In contrast, the elapsed time within each GNC mode is affected by the relative transitions into and out of that state. This is particularly useful for evaluating the accuracy with which these transitions are predicted.

The cumulative time in each GNC mode commander state was calculated from the telemetered state transition times. These cumulative times are reported in Table 4 and were compared to pre-flight Monte Carlo statistics. Table 4 provides the time difference between the flight value and the mean value from the Monte Carlo: $\Delta t_{flt} - mean\,(\Delta t_{sim})$. The final column in Table 4 expresses the flight measurement as a Gaussian quantile of the Monte Carlo data.

Table 5 summarizes the comparison between pre-flight simulation prediction of the GNC mode transition with the flight data. Some of the "$> 3.84\ \sigma$" results are due to very small differences in timing that are beyond the intended scope of the simulation. These differences arise due to conservative modeling of transport delays as well as fundamental differences between the asynchronous flight code and the synchronous simulation. These small timing differences are made obvious in fixed-duration modes such as "WAIT FOR BACKSHELL SEP" (mode 23), which is always precisely $1.4225\ s\ \pm 0.0\ s$ in the simulation. The observed flight time, $1.42188\ s$ is different by less than $1\ ms$, but is never-the-less smaller than the minimum in the simulation. Since the simulation was never intended to be that accurate, these instances – indicated by mean time differences on the order of one $64\ Hz$ sRTI or less – are of no concern. Other modes, specifically modes 4, 8, and 9, don't fall in this category. These modes ("RCS WARM UP," "WAIT FOR GUIDANCE START," and "RANGE CONTROL SLEW TO COMMANDED BANK ANGLE") indicate places where flight differed from simulation predictions, as described in the Early Guidance Start anomaly section (Section V.B).

D. GNC EVR Arguments

Similar to the timepoint firing and GNC mode transition, the pre-flight simulation recorded every argument to every GNC EVR created. For instance, the following "EDLGNC EVR TOUCHDOWN DETECTED2" EVR is produced at touchdown and has six arguments that provide direct, observable comparisons to the navigated state of the vehicle as reported in the flight EVR below.

```
"At Touchdown: Pos_Msf=[1493.940132 -1337.952938 19.215725] m,
 Vel_Msf=[-0.027829 0.002593 -0.513665] m/s"
```

The pre-flight simulation processed 422 individual similar metrics spanning multiple physical quantities, including: time, position, altitude, velocity, acceleration, attitude, attitude rate, and fuel use. This provided visibility into the performance of the simulation at critical events throughout the timeline. Ref. [12] lists the EVRs from flight and their

Table 4 Cumulative Time in Each GNC Mode.

		Flight (s)	Δ Mean (s)	Gauss. Quant. (σ)
4	RCS WARM UP	20.87500	0.375	> 3.8361
5	SPINDOWN	6.25000	0.078	0.7992
6	TURN TO ENTRY	11.25000	-9.599	-0.7443
7	WAIT FOR ENTRY	501.62500	9.021	0.6932
8	WAIT FOR GUIDANCE START	50.87500	-3.946	< −3.8361
9	RANGE CONTROL SLEW TO COMMANDED BANK ANGLE	6.25000	4.722	> 3.8361
10	RANGE CONTROL TRACK	51.62500	-3.575	-1.8120
11	RANGE CONTROL BANK REVERSAL	30.75000	3.030	1.1229
12	HEADING ALIGNMENT SLEW TO COMMANDED BANK ANGLE	6.50000	-0.335	-0.1107
13	HEADING ALIGNMENT TRACK	77.62500	0.243	0.0362
14	SLEW AND SUFR SLEW TO RADAR ATTITUDE	14.00000	0.270	0.7389
15	SLEW AND SUFR WAIT FOR CHUTE DEPLOY	3.00000	-0.270	-0.7389
16	ALLOW CHUTE DEPLOY TRANSIENTS TO SETTLE	10.01562	-0.000	< −3.8361
17	HEATSHIELD SEP LOGIC ENABLED	12.60938	2.279	1.2286
18	EDLGNC RCS CONTROL INHIBITED	3.01562	-0.109	< −3.8361
19	EDLGNC WAIT FOR TDS NAV INIT	2.10938	0.109	> 3.8361
20	TDS NAV INIT	29.12500	-0.459	-0.0490
21	MLE PRIMING LOGIC ENABLED	49.87500	5.265	0.8808
22	POWERED DESCENT START LOGIC ENABLED	8.75000	-0.363	-0.2415
23	WAIT FOR BACKSHELL SEP	1.42188	-0.001	< −3.8361
24	FREE FALL	0.96875	-0.016	< −3.8361
25	MLE WARM UP	0.21875	0.016	> 3.8361
26	PD DETUMBLE	0.14062	-0.107	-0.8966
27	PD TURN TO INITIAL ATTITUDE	0.93750	-0.175	-0.4988
28	PD POWERED APPROACH	29.71875	0.252	0.1835
29	PD CONSTANT VELOCITY ACCORDION	4.23438	0.084	0.1940
30	PD CONSTANT DECELERATION NOMINAL	5.89062	0.002	-0.4007
31	PD CONSTANT DECELERATION SATURATED AT MAX	0.00000	-0.008	< −3.8361
32	PD CONSTANT DECELERATION SATURATED AT MIN	0.00000	-0.007	< −3.8361
33	PD THROTTLE DOWN AND DAMP TRANSIENTS	2.53125	0.000	0.3184
34	PD DEPLOY ROVER AND DAMP TRANSIENTS	8.96875	-0.000	0.6640
35	PD READY FOR TOUCHDOWN	7.59375	0.268	0.4404
36	PD STOP VERTICAL MOTION	0.59375	0.000	0.6900
37	PD ALTITUDE HOLD	0.23438	0.000	-0.3161

Table 5 Summary of Time-in-Mode Comparisons

Range	Std. Normal	Count	Percentage
$\|\sigma\| > 3.84$	0.012%	11 of 34	32.35%
$3 < \|\sigma\| < 3.84$	0.258%	0 of 34	0.00%
$1.5 < \|\sigma\| < 3$	13.091%	1 of 34	2.94%
$\|\sigma\| < 1.5$	86.639%	22 of 34	64.71%

comparison with pre-flight estimates from the simulation. Table 6 shows a summary of the comparison between the pre-flight simulation and flight data. Similar to the GNC phase change, approximately 90% of the data were within $\pm 3\ \sigma$ of simulation predictions. Some of the cases that didn't fall within these bounds are discussed in Sec. V.

Table 6 Summary of EVR Comparisons

Range	Std. Normal	Count	Percentage
$\|\sigma\| > 3.84$	0.012%	31 of 422	7.35%
$3 < \|\sigma\| < 3.84$	0.258%	2 of 422	0.47%
$1.5 < \|\sigma\| < 3$	13.091%	39 of 422	9.24%
$\|\sigma\| < 1.5$	86.639%	350 of 422	82.94%

E. GNC Trajectory Reconstruction By Reverse Propagation

A Best Estimated Trajectory (BET) was constructed by the GNC team by back-propagating in-flight IMU measurements from the known landing location [4]. Table 7 lists trajectory data of this reconstruction [†] at critical events. Mars Orbiting Laser Altimeter (MOLA) altitudes, relative to the Mars areoid, and Above Ground Level (AGL) altitudes, relative to the Mars 2020 Digital Elevation Map (DEM), were obtained by querying simulation subroutines at the reconstructed inertial positions. Table 8 provides standard Gaussian quantiles for the as-flown values from Table 7, by comparing the as-flown values to the pre-flight Monte Carlo statistics. Table 9 summarizes the number and percentage of metrics within several quantile bins. Once again, the simulation performance for approximately 90% of statistics is within $\pm 3\sigma$, while the cases outside of those bounds fall in regions that are discussed in Sec. V.

Table 7 GNC Reconstructed Conditions.

Event	Time (s)	MOLA Alt (m)	AGL (m)	Rel. Vel. (m/s)	Long (deg)	Lat (deg)
RCS warm up	0.11	1421129.26	1421129.26	4684.34	30.66177	22.49165
Spindown	20.98	1358907.40	1358907.40	4709.26	31.64058	22.56972
Turn to entry	27.23	1340393.87	1340393.87	4716.94	31.93930	22.59210
Wait for entry	38.48	1307210.48	1307210.48	4730.66	32.48373	22.63121
Wait for guidance	540.11	128574.46	128574.46	5333.31	66.80017	20.82990
Range control	590.98	58750.91	58898.85	5355.17	71.33139	19.98815
1st bank reversal	621.86	25733.28	25337.18	4304.34	73.96318	19.40088
Peak deceleration	627.27	21887.44	22005.43	3777.37	74.32956	19.29670
End reversal 1	633.11	18940.45	18651.10	3202.36	74.67254	19.19920
2nd bank reversal	642.11	16059.48	16231.48	2454.90	75.10552	19.09525
End reversal 2	652.11	14644.30	14681.68	1877.04	75.47741	19.01881
3rd bank reversal	670.11	13957.31	14658.12	1284.98	75.95351	18.89299
Heading alignment	679.61	13917.97	14881.81	1098.68	76.14328	18.83234
End HA slew	686.11	13922.71	15013.36	1000.26	76.25848	18.79745
SUFR	763.73	11740.01	13796.43	487.96	77.15947	18.54326
Wait for PD	777.73	10392.26	12574.91	442.68	77.26793	18.51315
Parachute deploy	780.73	10039.04	12242.81	433.68	77.28951	18.50722
Peak inflation	782.40	9833.87	12086.33	423.72	77.30121	18.50400
HSS enabled	790.75	8976.58	11364.24	237.80	77.34290	18.49178
Heatshield sep.	803.61	7891.61	10379.55	158.10	77.37979	18.48083
Wait for NAV init.	806.38	7666.40	10116.49	148.23	77.38590	18.47913
NAV init.	808.48	7498.07	9961.09	141.48	77.39023	18.47790
TDS solution	837.61	4873.30	7386.49	102.77	77.42460	18.46726
LVS valid	879.12	1137.18	3699.29	86.89	77.43587	18.45267
MLE priming	887.48	430.15	2991.37	84.28	77.43776	18.45241
Wait for BSS	896.23	-286.21	2275.58	81.45	77.43976	18.45246
Free fall	897.66	-400.48	2161.14	81.10	77.44007	18.45240

Table 7 *Continued on the next page*

[†]Extracted from version v.3.2

Table 7 GNC Reconstructed Conditions. *Continued from the previous page.*

Event	Time (s)	MOLA Alt (m)	AGL (m)	Rel. Vel. (m/s)	Long (deg)	Lat (deg)
MLE warm up	898.62	-479.85	2081.88	84.55	77.44027	18.45235
Detumble	898.84	-498.22	2063.62	85.06	77.44032	18.45234
Turn to attitude	898.98	-510.07	2051.84	85.21	77.44035	18.45233
Powered approach	899.92	-589.15	1973.14	84.81	77.44054	18.45228
Constant velocity	929.64	-2314.29	254.25	32.38	77.45092	18.44464
Constant decel.	933.88	-2449.91	118.62	32.02	77.45091	18.44464
Throttle down	939.77	-2546.81	21.72	0.82	77.45091	18.44463
Deploy rover	942.30	-2548.71	19.82	0.65	77.45092	18.44463
Ready for TD	951.27	-2555.16	13.38	0.74	77.45092	18.44463
First contact	958.05	-2560.24	8.29	0.74	77.45092	18.44463
Touchdown detected	958.86	-2560.64	7.88	0.50	77.45092	18.44463
Altitude hold	959.45	-2560.77	7.76	0.06	77.45092	18.44463

Table 8 Comparing GNC Conditions to Sim. Predictions.

Event	Time (σ)	MOLA Alt (σ)	AGL (σ)	Rel. Vel. (σ)	Long (σ)	Lat (σ)
RCS warm up	> 3.84	< -3.84	< -3.84	> 3.84	> 3.84	> 3.84
Spindown	> 3.84	< -3.84	< -3.84	> 3.84	> 3.84	> 3.84
Turn to entry	2.84	-3.48	-3.48	2.86	3.48	> 3.84
Wait for entry	-0.69	0.68	0.68	-0.69	-0.68	-0.65
Wait for guidance	< -3.84	-1.79	-1.79	< -3.84	1.62	2.88
Range control	< -3.84	> 3.84	> 3.84	< -3.84	< -3.84	> 3.84
1st bank reversal	-0.82	1.26	1.35	0.56	-0.98	0.99
Peak deceleration	-0.57	0.83	0.82	0.58	-0.76	0.70
End reversal 1	-0.36	0.45	0.47	0.61	-0.49	0.50
2nd bank reversal	-0.63	0.34	0.35	0.48	-0.70	0.76
End reversal 2	-0.87	0.34	0.34	0.59	-0.85	0.78
3rd bank reversal	-0.93	0.48	0.42	1.07	-0.82	1.11
Heading alignment	0.23	0.51	0.53	-0.33	-0.35	-0.01
End HA slew	-0.08	0.55	0.55	0.21	-0.35	0.16
SUFR	0.02	1.07	1.07	1.16	0.82	-0.08
Wait for PD	0.10	1.12	1.16	1.44	1.62	-0.16
Parachute deploy	0.02	1.17	1.19	1.66	1.35	-0.09
Peak inflation	0.01	1.19	1.22	1.80	1.31	-0.08
HSS enabled	0.02	1.16	1.17	1.08	1.55	-0.19
Heatshield sep.	0.71	0.92	1.02	-0.04	1.49	-0.42
Wait for NAV init.	0.66	0.93	0.95	0.58	1.47	-0.41
NAV init.	0.71	0.92	0.95	0.76	1.50	-0.42
TDS solution	0.26	2.44	2.41	0.51	1.08	-0.42
LVS valid	0.56	-0.11	0.65	0.20	0.63	-1.11
MLE priming	0.53	-0.84	0.39	0.23	0.61	-1.04
Wait for BSS	0.47	-0.35	0.47	0.18	0.63	-0.97
Free fall	0.47	-0.42	0.53	0.18	0.63	-0.96
MLE warm up	0.47	-0.44	0.65	0.17	0.63	-0.96
Detumble	0.47	-0.49	0.60	0.15	0.63	-0.96

Table 8 *Continued on the next page*

Table 8 Comparing GNC Conditions to Sim. Predictions. *Continued from the previous page.*

Event	Time (σ)	MOLA Alt (σ)	AGL (σ)	Rel. Vel. (σ)	Long (σ)	Lat (σ)
Turn to attitude	0.47	-0.27	0.96	0.13	0.63	-0.96
Powered approach	0.46	0.02	0.93	0.10	0.64	-0.95
Constant velocity	0.45	-0.82	0.17	> 3.84	1.10	-1.46
Constant decel.	0.45	-1.28	-0.62	0.48	1.10	-1.46
Throttle down	0.45	-1.27	-0.65	0.65	1.10	-1.46
Deploy rover	0.45	-1.31	-1.34	-1.18	1.10	-1.46
Ready for TD	0.45	-1.27	-1.29	-0.17	1.10	-1.46
First contact	0.46	-1.29	< -3.84	-0.51	1.10	-1.46
Touchdown detected	0.46	-1.29	< -3.84	-3.23	1.10	-1.46
Altitude hold	0.46	-1.29	< -3.84	-1.27	1.10	-1.46

Table 9 Summary of GNC Comparisons

Range	Std. Normal	Count	Percentage
$\lvert\sigma\rvert > 3.84$	0.012%	25 of 234	10.68%
$3 < \lvert\sigma\rvert < 3.84$	0.258%	4 of 234	1.71%
$1.5 < \lvert\sigma\rvert < 3$	13.091%	12 of 234	5.13%
$\lvert\sigma\rvert < 1.5$	86.639%	193 of 234	82.48%

F. NewSTEP Trajectory Reconstruction By Kalman Filter

NewSTEP is an iterative extended Kalman filter (EKF) designed for post-flight trajectory reconstruction [5]. The EKF is formulated to blend various types of EDL measurement data to obtain the best estimate of the vehicle trajectory as well as uncertainty estimates of the reconstructed quantities. Estimates of the as-flown vehicle aerodynamic forces and moment coefficients are also produced. Table 10 lists trajectory data [‡] of this reconstruction at critical events. Table 11 provides standard Gaussian quantiles for the as-flown values from Table 10. Table 12 summarizes the number and percentage of metrics within several quantile bins. Although there are fewer cases in the $< 1.5\sigma$ category, about 90% of the statistics are within $\pm 3\sigma$. Upon inspection, the categories outside this region are again in areas covered in Sec. V.

Table 10 NewSTEP Reconstructed Conditions.

Event	Time (s)	MOLA (m)	AGL (m)	Rel Vel (m/s)	Atm Vel (m/s)	FPA (deg)	Mach	Dyn Pres (Pa)
RCS warm up	0.11	1421282.57	1421282.57	4684.39		-39.74		
Spindown	20.98	1359058.58	1359058.58	4709.18		-39.04		
Turn to entry	27.23	1340545.19	1340545.19	4716.94		-38.83		
Wait for entry	38.48	1307360.19	1307360.19	4730.66		-38.45		
Wait for guidance	540.11	128579.30	128579.30	5333.54		-16.18		
Range control	590.98	58741.75	58890.13	5355.41	5380.99	-13.31	26.93	511.09
1st bank reversal	621.86	25716.07	25309.36	4305.08	4285.97	-10.71	20.22	12784.32
Peak deceleration	627.27	21863.52	21982.53	3778.24	3758.20	-9.29	17.48	14507.33
End reversal 1	633.11	18911.97	18624.06	3203.05	3181.32	-7.61	14.56	13724.28
2nd bank reversal	642.11	16023.07	16195.98	2455.44	2431.89	-5.24	11.02	10563.03
End reversal 2	652.11	14607.80	14647.06	1877.60	1853.81	-2.49	8.33	6961.31
3rd bank reversal	670.11	13924.87	14623.41	1285.45	1263.93	-0.56	5.71	3511.32

Table 10 *Continued on the next page*

[‡]Extracted from version v.7

Table 10 NewSTEP Reconstructed Conditions. *Continued from the previous page.*

Event	Time (s)	MOLA (m)	AGL (m)	Rel Vel (m/s)	Atm Vel (m/s)	FPA (deg)	Mach	Dyn Pres (Pa)
Heading alignment	679.61	13888.53	14847.00	1099.11	1077.74	0.06	4.90	2591.34
End HA slew	686.11	13894.50	14990.12	1000.67	979.04	0.05	4.45	2137.18
SUFR	763.73	11733.14	13789.76	488.18	466.21	-9.55	2.09	588.39
Wait for PD	777.73	10390.54	12579.47	442.82	422.58	-14.89	1.86	530.42
Parachute deploy	780.73	10037.95	12247.04	433.88	414.22	-16.26	1.81	519.67
Peak inflation	782.40	9833.10	12088.05	424.10	404.78	-17.01	1.76	504.14
HSS enabled	790.75	8976.70	11363.76	237.78	220.31	-21.94	0.96	160.38
Heatshield sep.	803.61	7892.69	10378.32	158.18	144.90	-31.51	0.63	75.85
Wait for NAV init.	806.38	7667.76	10117.48	148.31	135.82	-32.82	0.59	67.88
NAV init.	808.48	7499.55	9962.50	141.60	129.72	-34.14	0.56	62.77
TDS solution	837.61	4876.98	7388.09	102.74	99.49	-69.63	0.42	45.60
MLE priming	887.48	434.84	2995.96	84.43	84.98	-81.06	0.35	47.54
Wait for BSS	896.23	-281.92	2279.98	81.50	82.34	-81.24	0.34	46.84
Free fall	897.66	-396.29	2165.44	81.26	82.14	-81.30	0.34	46.97
MLE warm up	898.62	-475.76	2085.84	84.72	85.58	-81.64	0.35	51.25
Detumble	898.84	-494.16	2067.43	85.24	86.10	-81.72	0.36	51.94
Turn to attitude	898.98	-506.03	2055.56	85.33	86.19	-81.79	0.36	52.08
Powered approach	899.92	-585.04	1976.97	84.85	85.68	-82.22	0.35	51.75
Constant velocity	929.64	-2311.75	256.61	32.20	32.78	-89.58	0.13	8.41
Constant decel.	933.88	-2447.75	120.60	32.14	32.76	-89.96	0.13	8.45
Throttle down	939.77	-2545.80	22.54	0.99	6.39	-85.70	0.03	0.32
Deploy rover	942.30	-2548.06	20.29	0.77	6.31	-86.72	0.03	0.31
Ready for TD	951.27	-2555.46	12.89	0.83	6.12	-81.27	0.02	0.30
First contact	958.05	-2561.06	7.26	0.82	6.07	-78.35	0.02	0.29

Table 11 Comparing NewSTEP Conditions to Sim. Predictions.

Event	Time (σ)	MOLA (σ)	AGL (σ)	Rel Vel (σ)	Atm Vel (σ)	FPA (σ)	Mach (σ)	Dyn Pres (σ)
RCS warm up	> 3.84	< -3.84	< -3.84	> 3.84		> 3.84		
Spindown	> 3.84	< -3.84	< -3.84	> 3.84		> 3.84		
Turn to entry	2.84	-2.90	-2.90	2.86		3.48		
Wait for entry	-0.69	0.69	0.69	-0.69		-0.68		
Wait for guidance	< -3.84	-1.59	-1.59	-0.57		-1.04		
Range control	< -3.84	> 3.84	> 3.84	< -3.84	-0.39	< -3.84	-0.44	-2.17
1st bank reversal	-0.82	1.24	1.27	0.57	0.55	-0.58	0.24	< -3.84
Peak deceleration	-0.57	0.80	0.80	0.59	0.55	-0.62	0.58	< -3.84
End reversal 1	-0.36	0.41	0.44	0.62	0.63	-1.22	0.44	1.07
2nd bank reversal	-0.63	0.30	0.32	0.48	0.50	0.01	0.51	0.75
End reversal 2	-0.87	0.30	0.30	0.60	0.62	0.27	0.50	0.43
3rd bank reversal	-0.93	0.45	0.39	1.08	1.06	0.42	0.93	1.00
Heading alignment	0.23	0.49	0.49	0.04	0.06	0.77	0.47	-0.04
End HA slew	-0.08	0.53	0.52	0.23	0.25	0.48	0.55	-0.02
SUFR	0.02	1.07	1.07	1.19	1.14	0.69	1.31	-0.00
Wait for PD	0.10	1.11	1.17	1.46	1.26	0.69	1.10	-0.10
Parachute deploy	0.02	1.16	1.20	1.69	1.42	0.80	1.08	-0.16

Table 11 *Continued on the next page*

Table 11 Comparing NewSTEP Conditions to Sim. Predictions. *Continued from the previous page.*

Event	Time (σ)	MOLA (σ)	AGL (σ)	Rel Vel (σ)	Atm Vel (σ)	FPA (σ)	Mach (σ)	Dyn Pres (σ)
Peak inflation	0.01	1.19	1.22	1.84	1.54	0.83	1.17	-0.09
HSS enabled	0.02	1.16	1.17	1.08	0.88	0.32	0.96	-0.02
Heatshield sep.	0.71	0.92	1.01	-0.01	-0.15	0.11	-0.14	-0.70
Wait for NAV init.	0.66	0.93	0.95	0.61	0.11	0.51	0.12	-0.49
NAV init.	0.71	0.92	0.95	0.78	0.28	0.66	0.28	-0.37
TDS solution	0.26	2.46	2.42	0.50	1.72	-0.87	3.17	1.66
MLE priming	0.53	-0.66	0.65	0.25	0.73	0.22	3.02	3.29
Wait for BSS	0.47	-0.26	0.59	0.19	0.66	0.91	2.59	3.48
Free fall	0.47	-0.32	0.68	0.20	0.70	1.00	2.84	3.66
MLE warm up	0.47	-0.34	0.84	0.20	0.69	1.01	2.82	> 3.84
Detumble	0.47	-0.38	0.79	0.18	0.64	1.01	2.59	3.37
Turn to attitude	0.47	-0.17	1.13	0.15	0.56	1.01	2.19	2.63
Powered approach	0.46	0.10	1.04	0.10	0.44	0.95	1.64	1.91
Constant velocity	0.45	-0.72	0.30	1.79	-0.08	0.37	-0.07	-0.06
Constant decel.	0.45	-1.20	2.36	3.66	-0.07	-2.10	-0.05	-0.05
Throttle down	0.45	-1.24	0.63	> 3.84	-1.01	-0.46	-1.00	-1.00
Deploy rover	0.45	-1.26	-0.52	1.77	-1.04	-0.93	-1.02	-1.02
Ready for TD	0.45	-1.31	-2.49	3.13	-1.09	1.30	-1.09	-1.09
First contact	0.46	-1.36	< -3.84	2.39	-1.10	2.15	-1.10	-1.10

Table 12 Summary of NewSTEP Comparisons

Range	Std. Normal	Count	Percentage
$\lvert\sigma\rvert > 3.84$	0.012%	21 of 273	7.69%
$3 < \lvert\sigma\rvert < 3.84$	0.258%	9 of 273	3.30%
$1.5 < \lvert\sigma\rvert < 3$	13.091%	29 of 273	10.62%
$\lvert\sigma\rvert < 1.5$	86.639%	214 of 273	78.39%

G. Atmospheric Comparison

Atmospheric properties were extracted from the wind-relative states in the NewSTEP BET [5] based on the compiled atmosphere [13]. Table 13 lists the atmosphere data [§] at critical events. Table 14 provides standard Gaussian quantiles for the as-flown values from Table 13 and Table 15 summarizes the number and percentage of metrics within several quantile bins. In the region where the pre-flight atmospheric model was based on mesoscale models (peak deceleration and below), the simulation compared well with the post-flight atmospheric model [13]. An exception was in the region of guidance start (range control), where the density was under-predicted. Ref [13] and Sec. V addresses this observation.

Table 13 NewSTEP Atmosphere Conditions.

Event	Pressure (Pa)	Temperature (K)	Density (kg/m^3)	Sound Speed (m/s)	Head Wind (m/s)
Range control	1.06	156.92	0.00004	199.79	25.58
1st bank reversal	46.90	176.63	0.00139	211.97	-19.11
Peak deceleration	71.25	181.80	0.00205	215.04	-20.04
End reversal 1	97.08	187.62	0.00271	218.46	-21.73

Table 13 *Continued on the next page*

[§] Extracted from NewSTEP version v.7 reconstruction and Compiled atmosphere v1

Table 13 NewSTEP Atmosphere Conditions. *Continued from the previous page.*

Event	Pressure (Pa)	Temperature (K)	Density (kg/m^3)	Sound Speed (m/s)	Head Wind (m/s)
2nd bank reversal	130.58	191.60	0.00357	220.77	-23.54
End reversal 2	150.57	194.81	0.00405	222.61	-23.78
3rd bank reversal	161.38	192.42	0.00440	221.24	-21.52
Heading alignment	162.07	190.39	0.00446	220.06	-21.37
End HA slew	162.04	190.47	0.00446	220.11	-21.62
SUFR	202.29	195.85	0.00541	223.20	-21.97
Wait for PD	230.51	203.39	0.00594	227.45	-20.24
Parachute deploy	238.37	206.26	0.00606	229.05	-19.66
Peak inflation	243.01	206.99	0.00615	229.46	-19.32
HSS enabled	263.29	208.84	0.00661	230.48	-17.46
Heatshield sep.	291.13	211.20	0.00723	231.78	-13.28
Wait for NAV init.	297.23	211.70	0.00736	232.06	-12.49
NAV init.	301.86	212.08	0.00746	232.26	-11.88
TDS solution	382.86	217.79	0.00921	235.37	-3.25
MLE priming	566.50	225.54	0.01317	239.52	0.55
Wait for BSS	602.53	228.58	0.01382	241.13	0.85
Free fall	608.45	229.08	0.01392	241.39	0.88
MLE warm up	612.58	229.43	0.01400	241.58	0.86
Detumble	613.54	229.51	0.01401	241.62	0.86
Turn to attitude	614.16	229.56	0.01402	241.65	0.86
Powered approach	618.30	229.91	0.01410	241.83	0.84
Constant velocity	714.19	239.16	0.01565	246.64	0.58
Constant decel.	722.14	240.45	0.01574	247.31	0.61
Throttle down	727.92	241.48	0.01580	247.84	5.40
Deploy rover	728.05	241.50	0.01580	247.85	5.54
Ready for TD	728.49	241.58	0.01581	247.89	5.29
First contact	728.82	241.64	0.01581	247.92	5.26

Table 14 Comparing NewSTEP Atmosphere to Sim. Predictions.

Event	Pressure (σ)	Temperature (σ)	Density (σ)	Sound Speed (σ)	Head Wind (σ)
Range control	-1.86	0.48	-2.15	0.42	-0.10
1st bank reversal	-1.60	0.07	-2.99	-0.00	0.04
Peak deceleration	-1.18	-0.06	-1.75	-0.12	-0.14
End reversal 1	0.06	0.03	0.02	-0.04	0.05
2nd bank reversal	-0.09	-0.06	0.13	-0.13	0.07
End reversal 2	-0.15	-0.03	-0.31	-0.10	0.04
3rd bank reversal	-0.18	-0.16	-0.13	-0.22	-0.01
Heading alignment	-0.34	-0.38	-0.12	-0.45	0.06
End HA slew	-0.55	-0.39	-0.49	-0.47	0.04
SUFR	-1.20	-0.42	-1.10	-0.50	-0.14
Wait for PD	-1.30	-0.13	-1.24	-0.20	-0.24
Parachute deploy	-1.24	-0.01	-1.38	-0.08	-0.26
Peak inflation	-1.19	0.01	-1.39	-0.07	-0.28
HSS enabled	-1.07	0.00	-1.25	-0.08	-0.32

Table 14 *Continued on the next page*

Table 14 Comparing NewSTEP Atmosphere to Sim. Predictions. *Continued from the previous page.*

Event	Pressure (σ)	Temperature (σ)	Density (σ)	Sound Speed (σ)	Head Wind (σ)
Heatshield sep.	-0.78	0.04	-0.96	-0.04	-0.15
Wait for NAV init.	-0.80	0.03	-0.98	-0.04	-0.16
NAV init.	-0.81	0.04	-0.97	-0.04	-0.16
TDS solution	-2.23	0.06	-0.81	-0.02	0.12
MLE priming	2.54	0.12	0.02	0.05	0.05
Wait for BSS	1.20	0.12	0.02	0.05	0.08
Free fall	1.58	0.12	0.02	0.05	0.08
MLE warm up	2.00	0.12	0.02	0.05	0.08
Detumble	2.17	0.12	0.03	0.05	0.08
Turn to attitude	1.88	0.12	0.02	0.05	0.08
Powered approach	1.17	0.12	0.01	0.04	0.08
Constant velocity	1.47	0.12	0.01	0.05	-0.10
Constant decel.	0.38	0.09	-0.00	0.02	-0.09
Throttle down	-0.04	0.08	-0.01	0.01	-1.07
Deploy rover	-0.02	0.08	-0.01	0.00	-1.06
Ready for TD	-0.01	0.08	-0.01	0.00	-1.11
First contact	-0.01	0.08	-0.01	0.00	-1.12

Table 15 Summary of Atmospere Comparisons

Range	Std. Normal	Count	Percentage
$\|\sigma\| > 3.84$	0.012%	0 of 93	0.00%
$3 < \|\sigma\| < 3.84$	0.258%	0 of 93	0.00%
$1.5 < \|\sigma\| < 3$	13.091%	11 of 93	11.83%
$\|\sigma\| < 1.5$	86.639%	82 of 93	88.17%

V. Anomalies

Some anomalies were identified during the statistical comparisons described in Sec. IV. All of these anomalies are considered minor, as they did not adversely affect the over-all EDL system performance or vehicle safety. The most significant is the over-prediction of peak deceleration, which is discussed in Section V.C.

A. Desynchronization of TZERO Events

The design of the MSL and Mars 2020 EDL sequence includes an anchor point, nominally 9 minutes prior to atmospheric Entry Interface (EI), known as TZERO. At this anchor, the GNC navigation dead-reckoning is initialized with a ground-commanded initial state. The SCLK time of this event and the initial state are included in the operational EDL Parameter Update (EPU) command. The SCET time of EI is provided by the navigation team and updated with each Orbit Determination (OD).

Due to the discrete nature in which the flight software operates on both 8 Hz Real-Time Interrupt (RTI) timing and 64 Hz Sub-RTI (sRTI) timing, the EDL team developed procedures to place the desired TZERO epoch at a SCET time that would coincide with both an 8 Hz SCLK tick and a 64 Hz SCLK tick. This requires knowledge of the error and drift of the onboard spacecraft clock. Ground tools use this knowledge to build an EPU command from the EDL team's desired TZERO SCET time, with an accuracy requirement of ± 1 ms.

In-flight, the allowable tolerance on the SCLK/SCET conversion resulted in a commanded SCLK time that was greater than the intended 8 Hz SCLK tick by less than 1 ms. Note that the scenario in which the actual time was greater than the desired time (a positive error), should have been expected with a likelihood of 50%. The consequence of this positive error was that actions that were performed on the 64 Hz bus were delayed 15.625 ms until the next sRTI, while

actions that were performed on the 8 Hz bus were delayed 125 ms until the following RTI. The magnitude of these delays was inconsequential to the operation of the EDL timeline and there was no impact to EDL system performance. However, actions that were expected to be synchronized between the two rate groups occurred in-flight at slightly different times. The actual flight times of these events are listed in Table 16.

Table 16 Multiple TZEROs

SCLK Time	Description	Notes
666951979.500000	Targeted RTI	Both 8 Hz and 64 Hz aligned
666951979.500504	Actual EPU command	Within required ±1 ms tolerance of above
666951979.515625	Next 64 Hz sRTI	Timeline engine timepoints
666951979.625000	Next 8 Hz RTI	GNC mode commander transition

By choice, the simulation does not directly model a spacecraft clock that is different and independent from the simulation time. Because of this, simulation time is always initialized in a manner that enforces synchronization of the 8 and 64 Hz software buses. This results in slight differences in time-fixed event timings (on the scale of an RTI), that are beyond the minimum or maximum captured in the pre-flight simulations as was discussed in Sec. IV.B. This does not result in degraded EDL system performance or margins, but is still preventable, and currently does not allow the simulation to reflect flight-like conditions. One potential recommendation to reconcile a non-deterministic flight behavior is to include rounding the commanded TZERO SCLK time to the nearest RTI when building the EPU flight product, or changing the ground SCLK/SCET tolerance to $\pm 1ms$.

B. Early Guidance Start

Following EI, the EDL sequence must delay the start of entry guidance's active bank control until sufficient control authority has been established. This is the first trigger in the EDL sequence to use in-situ measurements from on-board sensors to react to the environment of Mars. This trigger fires when the filtered drag acceleration exceeds 0.2 Earth g [14]. Prior to this point, the attitude of vehicle is held at a pre-determined bank angle based on the expected bank command from entry guidance.

In flight, this trigger fired approximately 4 s earlier than predicted, and at a higher altitude and longer range to the target. Figure 8 compares the predicted and actual guidance start time. The calculated bank angle at these conditions (36.175404 deg) was significantly more lift-up than the established pre-bank angle (73.705429 deg), due to the larger than expected range-to-go. This led to a large 37.53 deg programmed slew to the entry guidance commanded attitude and the issuance of an off-nominal "RANGE CONTROL OFF NOM 4" X-band semaphore. However, this higher-than-expected commanded lift persisted for only the first 10 to 12 seconds, until the commanded bank angle returned to pre-flight levels. There was minimum impact on EDL performance and timeline and led to perhaps 1-2 kg more fuel usage.This behavior is discussed in more detail in the guidance section of Ref. [12].

The cause of the anomaly is an under-prediction of the atmospheric drag experienced in the upper atmosphere (above 50 km). In flight, the vehicle experienced a denser than modeled atmosphere and therefore, reached the sensed acceleration threshold at a higher altitude. A similar behavior, though not nearly as severe, occurred on MSL [11]. The rationale behind the under-prediction is described in Ref. [13].

The reason for a lack of sensitivity to this under-prediction is two-fold. First, very little of the total deceleration during EDL occurs at altitudes above 40 km, so there is no expectation that mis-modeled atmosphere in this region would result in significant performance impacts. Second, entry guidance is specifically designed to compensate for these types of differences in acceleration, in order to ensure the desired terminal condition are met. This is the exact purpose of flying closed-loop entry guidance.

While the magnitude of the error was larger for Mars 2020 than MSL, the EDL team again observed no detrimental effects on EDL performance. One could argue that due to this lack of sensitivity, significant resources need not be expended to correct these errors on future flights. However, an additional source of atmospheric data – historical MCS temperature profiles – specific to Mars 2020's landing site and season, and valid to altitudes as high as 90 km, were available to the EDL team but were not used for this purpose. Post-flight analysis shows that incorporating this information into the simulation captures the observed, as-flown behavior. Due to this readily available information, it is recommended that an upper atmosphere model based on historical MCS temperature profiles should be used [13].

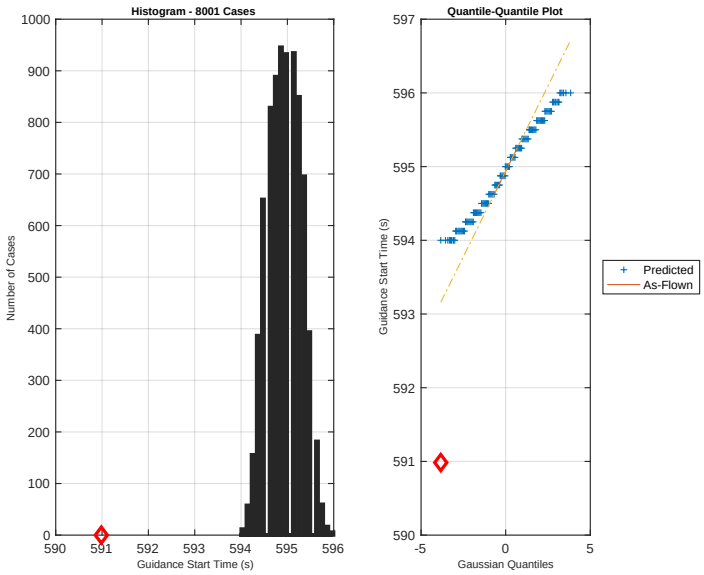

Fig. 8 Guidance Start Time.

C. Over-prediction of Peak Deceleration

A surprising anomaly was the over-prediction of peak deceleration during EDL. The observed peak deceleration in-flight (10.73 g's) was approximately 0.25 g's lower than pre-flight Monte Carlo bounds. Figure 9 compares the as-flown peak deceleration to pre-flight predictions. While lower than expected deceleration is not a worrisome issue for the EDL system, it was initially unclear why the simulation did not capture this possibility. Pre-flight, the EDL team was particularly interested in the simulation's peak deceleration prediction. The project needed to reduce the flight limit load (FLL) of the heatshield after a failed structural test during an over test. The EDL team lowered the FLL from 15 g's to 12 g's. This reduced the required static test loads for the new heatshield, but at the expense of a perceived reduction of operational margins.

The under-prediction of peak deceleration was puzzling given that flight conditions at peak deceleration were well within simulation predictions. Time, altitude, velocity, and flight path angle were all within 1 σ. Likewise, atmospheric properties were also well predicted: Temperature, speed of sound, Mach number, and wind speed were all within 1 σ, while pressure and density were within 1 σ to 2 σ. However, the reconstructed dynamic pressure ($14,507\ Pa$) was $93\ Pa$ less than the minimum Monte Carlo case of $14,600\ Pa$. As seen in Figure 10, although atmospheric relative velocity and density were within pre-flight predictions, they were correlated and the as-flown values of the dynamic pressure and the correlated density and velocity were outside the predicted range. Thus, it is important to understand what was mis-predicted in the physics captured within the simulation.

Looking at simplified 2-dimensional, planar, equations of motion can shed some light on the subject. The magnitude of the deceleration ($\dot{V}$) can be framed as a function of the instantaneous flight conditions. Differentiating the acceleration provides an expression for the jerk ($\ddot{V}$), which will be set to zero to solve for the local maximum of the acceleration. Considering only the aerodynamic deceleration due to drag forces, one can write the acceleration (Equation 3) as the dynamic pressure (q) divided by the ballistic coefficient (β). This approach neglects the effects of aerodynamic lift, gravity, Reaction Control System forces, and centrifugal, Coriolis, and Euler accelerations, but for EDL drag is the prime driver. This leads to a result that is not exact but illustrative of the conclusions drawn from a more detailed analysis.

$$\dot{V} = \frac{q}{\beta} = \frac{1}{\beta}\left(\frac{1}{2}\rho V^2\right) \tag{3}$$

Assuming a constant ballistic coefficient, we see that the jerk (Equation 4) is a function of derivatives of the components of dynamic pressure, namely density (ρ) and velocity (V). As the vehicle decelerates, the atmosphere becomes more dense faster than the velocity is reduced, but at peak deceleration, these two effects are perfectly balanced, resulting in zero jerk. Solving for acceleration at this point, the expression for peak deceleration is in Equation 5.

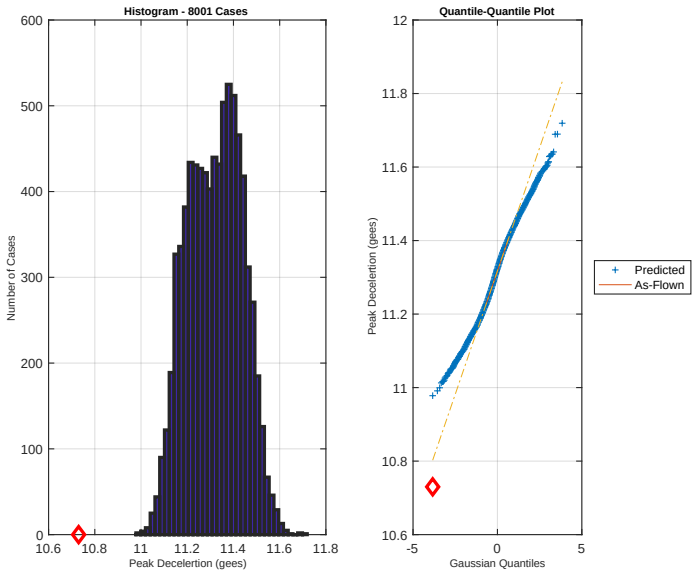

Fig. 9 Peak Deceleration.

$$\frac{\ddot{V}}{\dot{V}} = \frac{\dot{\rho}}{\rho} + 2\frac{\dot{V}}{V} \tag{4}$$

$$\dot{V}_{max} = -\frac{1}{2}V\left(\frac{\dot{\rho}}{\rho}\right) \tag{5}$$

Peak deceleration is not only dependent on the instantaneous value of density (ρ), but also its slope ($\dot{\rho}$) – which is a function of the modeled atmospheric profile. Assuming an ideal gas equation of state (Equation 6), we can write an expression for the time derivative of density ($\dot{\rho}$) in terms of the slope of the pressure profile, with respect to altitude, (dP/dh) and the temperature lapse rate (dT/dh) – both of which are typically negative in this region of the atmosphere. Substituting Equation 7 into Equation 5 and altitude rate ($\dot{h} = Vsin\gamma$), results in Equation 8 for peak deceleration.

$$\rho = \frac{P}{RT} \tag{6}$$

$$\frac{\dot{\rho}}{\rho} = \left[\frac{1}{P}\left(\frac{dP}{dh}\right) - \frac{1}{T}\left(\frac{dT}{dh}\right)\right]\dot{h} \tag{7}$$

$$\dot{V}_{max} = -\frac{1}{2}V^2 sin\gamma\left[\frac{1}{P}\left(\frac{dP}{dh}\right) - \frac{1}{T}\left(\frac{dT}{dh}\right)\right] \tag{8}$$

A larger scale height (less negative dP/dh) leads to lower deceleration, which is consistent with the compiled atmosphere from flight [13]. Also, a larger lapse rate (more negative dT/dh) likewise leads to a lower deceleration. However, this is inconsistent with the as-flown atmosphere profile, which shows a lower lapse rate than the pre-flight model. Therefore, a likely cause of the peak deceleration anomaly was an under-prediction of the pressure scale height. Ref. [13] discusses how this could be rectified in a future atmospheric model.

D. Under-prediction of MLE Performance

The in-flight MLE performance was reconstructed to be higher than the pre-flight predictions. One indication is a further than predicted fly-away distance, as shown in Figure 6. Since the flyaway burn is open-loop, a larger thrust-to-mass ratio will result in a longer distance flown. The second indication is a consistent pattern of large powered descent controller vertical position errors throughout powered descent [4]. Table 17 lists the position errors reported via EDL GNC EVRs, along with the 99 percentile pre-flight estimates, and the relative Gaussian quantiles of the as-flown values.

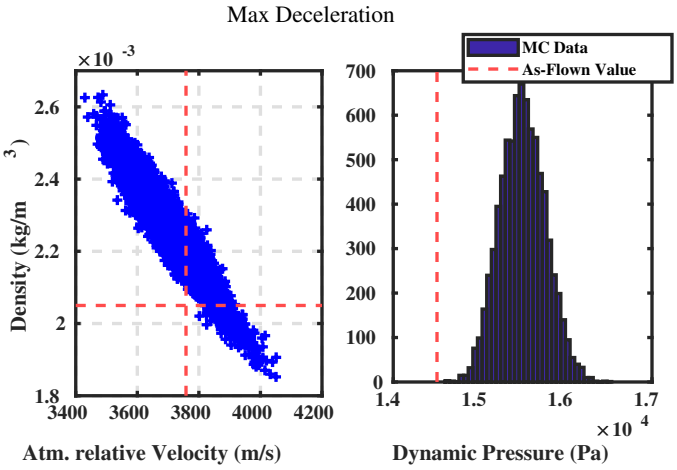

Fig. 10 Atmospheric relative quantities at peak deceleration.

Table 17 Vertical Position Errors Reported During Powered Descent.

Powered Descent Event	As-Flown Pos. Err. (m)	Simulated 99%-tile (m)	Gaussian Quantile (σ)
Constant Velocity	0.059	0.039	> 3.836
Constant Deceleration	0.059	0.036	> 3.836
Throttle Down	0.103	0.077	> 3.836
Rover Separation	0.054	0.045	> 3.836
Ready for Touchdown	0.035	0.025	> 3.836

This consistent over-shoot of the targeted altitudes can be explained by a higher MLE thrust for a given commanded pintle position. The EDL GNC reconstruction team estimated that a bias of approximately 95 N of thrust per engine could explain these observed anomalies [4]. The root cause of this over-performance is still under investigation by the propulsion team.

Note that while the as-flown values of the position errors exceeded pre-flight predictions, the magnitude of these errors (3 to 10 cm) is very small compared to the available 5 m touchdown accordion, which is included in the design of the powered descent profile. Likewise, the magnitude of the estimated bias in thrust is very small compared to full the capability of the engines (3200 N). Therefore, these position errors did not contribute any appreciable risk to the safety of the system.

VI. Lessons Learned

Overall the EDL simulation performed very well, as quantified by successfully predicting over 90% of the flight metrics compared in Section IV to within $\pm 3\,\sigma$ of the mean prediction. However, aside from this being a high percentage, that statistic does not tell us if the underlying models are all good representation of the truth. From the remaining 10% of metrics, three minor anomalies were identified, which were discussed in the previous subsections. None of these anomalies significantly impacted the vehicle performance or adversely jeopardized the safety of the landing. The most significant of these was the over-prediction of the peak deceleration, which would have been more serious had the flight load been higher than predicted, rather than lower.

The fact that these anomalies had little impact on over-all vehicle performance can be attributed to an appropriate expenditure of resources to risk mitigation by the EDL team throughout system development. In general, the simulation predictions were more accurate in the high-sensitivity areas where close attention was paid, and less accurate in the low-sensitivity areas that were given the least attention. In this regard, the safe landing and the over-all good performance of the simulation validates the models, methodologies, and philosophies used to develop the simulation and to design, validate, and operate the EDL system.

Nevertheless, some improvements are warranted. The most significant lesson learned is the difficulty in bounding

the atmospheric environment. It was demonstrated by the peak deceleration anomaly that the current pre-flight model is insufficient to bound the expected density, temperature, and pressure. The derivatives of these quantities must also be considered: the density and pressure scale heights and the lapse rate. The simulation's atmosphere model should provide sufficiently conservative uncertainties in these derivatives to bound the expected environmental conditions. With regards to upper atmosphere modeling (altitudes above 50 km) the team failed to utilize the available historic MCS data, which lead to the early guidance start anomaly. Middle atmosphere modeling (altitudes between 20 to 50 km) suffered from the introduction of a bias in scale height, caused by averaging disagreeing mesoscale model predictions, which resulted in the peak deceleration anomaly. However, the lower atmosphere predictions (altitudes below 20 km), which were the most important to EDL performance, were very accurately predicted, resulting in very good predictions of critical altitude and timeline margins and accurate targeting. Some further discourse of improvements to the atmospheric model are presented in Ref. [13].

VII. Summary

The Mars 2020 spacecraft successfully landed the Perseverance rover and Ingenuity helicopter on Feb. 18, 2021. The pre-flight simulation provided predictions of the entry, descent, and landing phase of flight and these predictions compared well with the post-flight reconstruction of flight conditions. Approximately 90% of the EDL as-flown values were within the $\pm 3\sigma$ of the pre-flight simulation metrics, but small anomalies were observed in some areas of the flights. Specifically, the entry guidance started 4 s early due to under-prediction of the density in the upper atmosphere and the peak acceleration was overpredicted, which post-flight analysis suggests were due to under-prediction of the density and pressure scale height. Approaches for suggested updates for the atmospheric modeling were discussed to improve the overall EDL simulation performance for a future flight.

Acknowledgments

The authors want to thank the Mars 2020 EDL team who helped with the modeling of most segments of the simulation.

References

[1] Way, D., "On the Use of a Range Trigger for the Mars Science Laboratory Entry, Descent, and Landing," IEEE AC 1142, *IEEE Aerospace Conference,* Big Sky, MT, 2011.

[2] Dutta, S., and Way, D., "Comparison of the Effects of Velocity and Range Triggers on Trajectory Dispersions for the Mars 2020 Mission," AIAA 2017-0245, *AIAA Atmospheric Flight Mechanics Conference,* Grapevine, TX, 2017.

[3] Mohan, S., Johnson, A., Brugarolas, P., Cheng, Y., Otero, R., Trawny, N., Aaron, S., Serrichio, F., Montgomery, J., Casoliva, J., and Chen, A., "Assessment of M2020 Terrain Relative Landing Accuracy: Flight Performance vs. Predicts," AAS 21-541*, AAS/AIAA Astrodynamics Specialist Conference,* Big Sky, MT, 2021.

[4] Serrichio, F., San Martin, A., Brugarolas, P., and Casoliva, J., "The Mars 2020 Perseverance Navigation Filter," AAS 21-539*, AAS/AIAA Astrodynamics Specialist Conference,* Big Sky, MT, 2021.

[5] Karlgaard, C., Schoenenberger, M., Dutta, S., and Way, D., "Mars Entry, Descent, and Landing Instrumentation 2 Trajectory and Atmosphere Reconstruction," *AIAA SciTech 2022, AIAA Atmospheric Flight Mechanics Conference,* San Diego, CA, 2022.

[6] Braun, R. D., Powell, R. W., Engelund, W. C., Gnoffo, P. A., Weilmuenster, K. J., and Mitcheltree, R. A., "Mars Pathfinder Six-Degree-of-Freedom Entry Analysis," *Journal of Spacecraft and Rockets*, Vol. 32, No. 6, 1995, pp. 993–1000. doi: 10.2514/3.26720.

[7] Desai, P. N., Schoenenberger, M., and Cheatwood, F. M., "Mars Exploration Rover Six-Degree-of-Freedom Entry Trajectory Analysis," *Journal of Spacecraft and Rockets*, Vol. 43, No. 5, 2006, pp. 1019–1025. doi:10.2514/1.6008.

[8] Desai, P. N., Prince, J. L., Queen, E. M., Schoenenberger, M., Cruz, J. R., and Grover, M. R., "Entry, Descent, and Landing Performance of the Mars Phoenix Lander," *Journal of Spacecraft and Rockets*, Vol. 48, No. 5, 2011, pp. 798–808. doi:10.2514/1.48239.

[9] Way, D. W., Davis, D., Jody, and Shidner, J. D., "Assessment of the Mars Science Laboratory Entry, Descent, and Landing Simulation," AAS 13-420*, AAS/AIAA Space Flight Mechanics Conference,* Kauai, HI, 2013.

[10] Maddock, R., Cianciolo, A., Korzun, A., Litton, D., Zumwalt, C., and Karlgaard, C., "InSight Entry, Descent, and Landing Postflight Performance Assessment," *Journal of Spacecraft and Rockets*, Vol. 58, No. 5, 2021, pp. 1530–1537. doi:10.2514/1.A35023.

[11] Chen, A., Cianciolo, A., Vasavada, A., Karlgaard, C., Barnes, J., Cantor, B., Kass, D., Rafkin, S., and Tyler, D., "Reconstruction of Atmospheric Properties from Mars Science Laboratory Entry, Descent, and Landing," *Journal of Spacecraft and Rockets*, Vol. 41, No. 4, 2014, pp. 1062–1075. doi:10.2514/1.A32708.

[12] Chen, A., et al., "Mars 2020 Entry, Descent, and Landing As-Flown Report," Tech. rep., Jet Propulsion Laboratory, Pasadena, CA, 2021, in work.

[13] Dutta, S., Karlgaard, C., Kass, D., Villar, G., and Mischna, M., "Post-flight Analysis of Atmospheric Properties from Mars 2020 Entry, Descent, and Landing," *AIAA SciTech 2022, AIAA Atmospheric Flight Mechanics Conference,* San Diego, CA, 2022.

[14] Mendeck, G., and McGrew, L., "Entry Guidance Design and Postflight Performance for 2011 Mars Science Laboratory Mission," *Journal of Spacecraft and Rockets*, Vol. 51, No. 4, 2014, pp. 1094–1105. doi:10.2514/1.A32737.